Relating solute and gas dispersion in gravel at different transport velocities

L. Pugliese[1], T. G. Poulsen[1] & S. Straface[2]
[1]*Department of Chemistry and Biotechnology, Aalborg University, Denmark*
[2]*Department of Ingegneria per l'Ambiente, il Territorio e Ingegneria Chimica, Universita' della Calabria, Italy*

Abstract

Dispersion is a key process controlling transport of solutes and gases in porous media. Performing tracer tests for dispersion measurements with solutes is generally much more time consuming compared to used gases. The goal of this study is to estimate the solute dispersion based on gas dispersion measurements to reduce time consumption. Solute (chloride ion) breakthrough curves were measured at different fluid velocities, covering the identical Reynolds range used in a previous study on gas dispersion. Commercial gravel, consisting of solid particles, has been used as a porous medium. Chloride and oxygen dispersion coefficients were determined based on the measured breakthrough data and in turn used to calculate solute and gas dispersivities as a function of the particle size (D_m) and particle size range (R). Solute dispersivity increased with increasing particle size range, in agreement with the previous study. Data showed that dispersivity increases more gradually with decreasing mean diameter.
Keywords: solute dispersion, gas dispersion, dispersivity ratio, porous medium, Reynolds number, particle size range.

1 Introduction

Movement of solutes and gases in a porous media is controlled by fluid phase advection, molecular diffusion and mechanical dispersion. Dispersion in solute is important in case of contaminant transport in both saturated and unsaturated soil [1–3], as well as nutrient transport in the root zone [4]. Gas phase dispersion


WIT Transactions on Engineering Sciences, Vol 79, © 2013 WIT Press
www.witpress.com, ISSN 1743-3533 (on-line)
doi:10.2495/MPF130281

controls processes such as radon migration into buildings [5], soil aeration and movement of volatile contaminants for instance at contaminated soil sites [6, 7]. Gas dispersion also plays an important role for processes such as migration and emission of methane (and other volatile compounds) at landfills, methane emissions from wetlands [8–13] and oxygen and CO_2 movement in passively aerated compost piles [14, 15].

Dispersion in porous media has been investigated for several decades, since the 1960. These studies focused chiefly on physical parameters, such as fluid phase velocity, fluid filled porosity and particle size distribution [16–21]. Accurate studies on gas dispersion were first introduced in the late 1960s [22–28]. An excellent review of the existing knowledge about dispersion of solutes and gases in homogeneous porous media has been published from Delgado [29]. This and later studies [28, 30–33] confirmed that dispersion increases with fluid phase velocity, distance travelled, particle shape deviation from spherical, particle size range, and pore system tortuosity.

A large number of researches on solute dispersion in both artificial and natural porous media is available into literature [34–38]. On the contrary, the majority of studies on gas dispersion are mainly related to artificial media. Despite this, the parameters affecting solute and gas dispersion are the same and they affect both gas and solute dispersion in a similar manner.

Measurements using gases as tracers, through a porous media, are much faster of those using solutes. In coarse-grained materials, such as sand, this difference is equal to 10-100 times under identical conditions. In finer grained material, such as fine sand and silt, the difference might be even larger. At present, however, no studies focusing on corresponding measurements of liquid and gas dispersion coefficients, in identical natural porous media, have been published. Therefore the identification of the link between gas and solute dispersion has not yet been obtained. The objective of this study was to investigate solute and gas dispersion, in a natural media under identical conditions. A simple relationship among the two tracers, yielding considerable time savings, was found. Solute measurements were carried out using NaCl as it is cheap, simple and safe to use. Gas measurements belong to a previous study [32], based on the same procedure but using O_2 as a tracer.

2 Theory

Transport in porous media is generally described by the advection dispersion equation (ADE). For one-dimensional transport of a conservative tracer in a column containing homogeneous porous medium, under assumption of uniform flow and dispersion, and the presence of both a mobile and a immobile fluid phase, the ADE is given as:

$$\frac{\partial C_m}{\partial_t} = D\frac{\partial^2 C_m}{\partial x^2} + u\frac{\partial C_m}{\partial x} + \tau(C_{im} - C_m) \quad (1)$$

where C_m and C_{im} are the tracer concentrations in the mobile and immobile fluid phases (kg m^{-3}), D is the overall dispersion-diffusion coefficient (m^2 s^{-1}), u is the

pore fluid velocity (interstitial velocity) in the mobile phase (m s^{-1}), τ is the tracer mass transfer coefficient (s^{-1}) for mass transfer between the mobile and immobile fluid phases, and x and t are the space (m) and time variables (s) [32].

Tracer concentration for the immobile fluid phase is expressed as:

$$\frac{\partial C_{im}}{\partial_t} = -\frac{\varepsilon_m}{\varepsilon_{im}}\tau(C_{im} - C_m) \tag{2}$$

where ε_m and ε_{im} are the mobile and immobile volumetric phase contents (m^3 m^{-3}) in the porous medium, respectively. The immobile fluid phase content and the fluid pore velocity are calculated as:

$$\varepsilon_{im} = \varepsilon_{tot} - \varepsilon_m \tag{3}$$

$$u = -\frac{Q}{A\varepsilon_m} \tag{4}$$

where ε_{tot} is the total fluid-filled porosity (assumed equal to medium total porosity), Q is the applied volumetric fluid flow rate (m^3 s^{-1}), and A is the column cross-sectional area (m^2) perpendicular to the fluid flow direction. In case of a medium without an immobile fluid phase the tracer transport process is described by eqns. (1), (2) and (4) with τ equal to zero and ε_m equal to the total fluid phase filled porosity. D can be expressed as:

$$D = D_{diff} + D_{mech} \tag{5}$$

where D_{diff} represents the contribution by molecular diffusion and D_{mech} the contribution from mechanical dispersion. Assuming for a one-dimensional configuration that D_{mech} increases linearly with increasing fluid flow pore velocity [28, 32, 39, 40] we obtain:

$$D_{mech} = u\alpha \tag{6}$$

where α is the tracer mechanical dispersivity in the mobile fluid phase (m). Combining eqns. (5) and (6) yields:

$$D = D_{diff} + \alpha u \tag{7}$$

A straight line characterizes the plot of D versus u, identified by the slope α and the intercept D_{diff}, except at very low fluid flow velocities [28].

3 Materials and methods

Measurements of gas and liquid phase dispersion coefficients were carried out using, as a porous medium, commercially available gravel. Particles were sieved into fractions with 2 mm particle size range (R = 2), and particle diameter (D) of 2–4, 4–6, 6–8, 8–10, 10–12 and 12–14 mm, corresponding to a mean particle diameter (D_m) of 3, 5, 7, 9, 11, 13. Combining these 2 mm fractions additional particle size fractions were produced having R = 4 mm (D_m = 4, 6, 8, 10, 12), R = 6 mm (D_m = 5, 7, 9, 11), R = 8 mm (D_m = 6, 8, 10), R = 10 mm (D_m = 7, 9), R = 12 mm (D_m = 8). A uniform particle size distribution was achieved by using

equal masses of each 2 mm particle size fraction. A total of 21 particle size fractions were produced. The gravel was packed into clear acrylic columns 100 cm in length and 14 cm inner diameter. Packing was conducted taking care to reduce differences in packing density of each column. Physical particle properties are shown in table 1.

Table 1: Properties of gravel used in the measurements of dispersion.

Particle size (mm)	ρ_b (g/cm^3)	ε_{tot} (cm^3/cm^3)	$D_{diff\text{-}gas}$ (cm^2/min)	α_g (cm)	α_w (cm)	α_g/α_w (cm/cm)
2-4	1.55	0.42	4.55	0.38	0.68	0.56
2-6	1.54	0.42	4.52	0.79	-	-
2-8	1.56	0.41	3.75	1.24	0.58	2.15
2-10	1.59	0.40	4.22	1.88	-	-
2-12	1.58	0.40	3.63	2.08	-	-
2-14	1.61	0.39	4.17	2.55	0.79	3.22
4-6	1.54	0.42	4.02	0.46	-	-
4-8	1.53	0.42	4.30	1	-	-
4-10	1.54	0.42	3.80	1.34	-	-
4-12	1.58	0.40	3.65	1.8	0.47	3.81
4-14	1.59	0.40	3.64	2.03	-	-
6-8	1.54	0.42	3.82	0.51	0.60	0.85
6-10	1.54	0.42	4.03	0.91	0.67	1.35
6-12	1.55	0.42	3.90	0.78	-	-
6-14	1.56	0.41	3.85	1.32	-	-
8-10	1.55	0.42	4.38	0.61	0.34	1.79
8-12	1.56	0.41	3.85	0.71	-	-
8-14	1.56	0.41	3.96	1.07	0.36	2.96
10-12	1.55	0.42	4.30	1.18	-	-
10-14	1.55	0.42	3.88	0.78	-	-
12-14	1.55	0.42	4.53	0.94	0.28	3.41

Soft Teflon tubing (inner diameter 4 mm) was used to connect system components. A 1 mm aluminium sheet with 2 mm opening was installed at both ends of the column to prevent movement of the media. Different flow rates were used for both solute and gas measurements in order to obtain comparable results covering the same Reynolds range ($0.04 \leq Re \leq 2.13$).

Measurements of solute dispersion were carried out using a peristaltic pump connected to the bottom of the column (inlet). The outlet was connected to a

measuring tube holding 12 ml of liquid, equipped with a TETRACON 925 conductometer. A schematic of the experimental set-up is shown in fig. 1.

Due to the high time consumption only 9 out of 21 fractions were used for the measurements. After flushing the column with demineralized water at a certain flow, a NaCl (5 g l^{-1}) solution was injected at the same flow. Effluent NaCl concentration was logged every 10 seconds using a data logger (Multi3420, WTW®, Herlev, Denmark). Breakthrough curves for NaCl replacing demineralized water were measured for gas flow rates of 0.015, 0.5, 0.075, 0.1, 0.125, 0.15 l/min in duplicate. Measurements were terminated when in and outlet NaCl concentrations were identical.

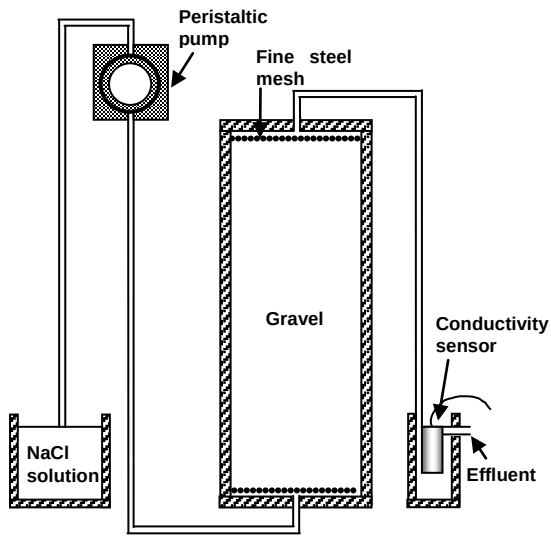

Figure 1: Experimental set-up for measurements of NaCl.

Gas dispersion data were taken from Sharma [32], following the approach of Poulsen [28]. O_2 breakthrough curves were measured in duplicate at gas flow rates of 0.2, 0.5, 1.0, 1.5, and 2 l/min. All 21 fractions were used for the measurements.

The measured breakthrough curves were fitted to eqns. (1)–(4) by optimizing the values of D, τ and ε_m. Initial conditions for the solute and gas transport simulations were:

$$t = 0, x \geq 0 \qquad C = 0 \tag{8}$$

Boundary conditions for the solute and gas transport simulations were:

$$t > 0, x = 0 \qquad C = C_0 \tag{9}$$

Eqns. (1)–(4) were solved using an explicit finite difference method, corrected for numerical dispersion. Optimum values of D, τ and ε_m for each of the 318 measured gas and liquid breakthrough curves were determined by

minimizing the sum of squared errors (SSE) between measured effluent tracer concentrations and corresponding tracer concentration values predicted by the numerical model as:

$$SSE = \sum_{t=0}^{t\,max} \left[C_{measured}(t) - C_{predicted}(t)\right]^2 \quad (10)$$

where $C_{measured}$ (t) and $C_{predicted}$ (t) are the observed and predicted (by the model) effluent tracer concentration at time t, respectively, while t_{max} is the time at which each individual experiment was terminated. The minimization procedure was carried out using a non-linear least square method.

4 Results and discussion

Selected measured NaCl breakthrough curves for the 6-8 mm particle fraction are shown in fig. 2(a). The four curves, representing four different flow rates, all exhibit a sigmoid shape generally expected for this type of experiments. Similar trend was identified for all the 108 breakthrough curves (solute measurements). A small tailing, indicating the presence of an immobile solute phase, is mainly exhibited at low flow rates (< 0.075 l min^{-1}) and in the upper part of the curves (near C/C_0=1). Fig. 2(b) shows selected O_2 breakthrough curves for the 6-8 mm particle fraction. Curves are not completely symmetrical but exhibit some little tailing, indicating the presence of an immobile gas phase ($\tau > 0$) for some experiments. This was the case for Q ≤ 0.5 l min^{-1} indicating that all air was mobile above this flow rate. A typical sigmoid shape is also exhibit for all gases measurements (210). Comparing flow and pressure gradients for all solute and gas data, shows that under identical conditions and for identical Re number, measurements of the solute breakthrough curves takes 12 times longer than for the gas.

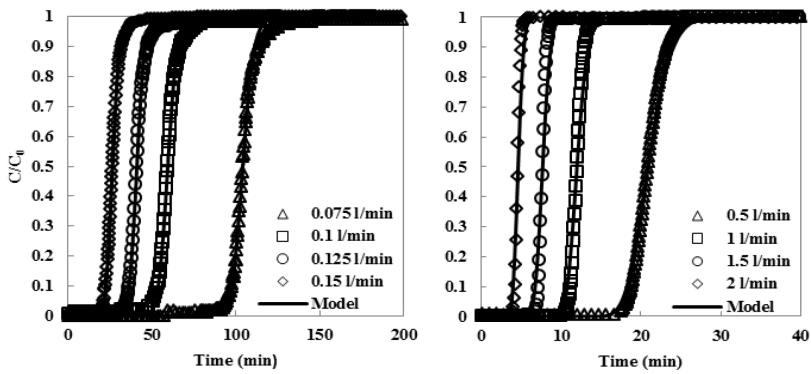

(a) (b)

Figure 2: Measured and fitted values of effluent NaCl (a) and O_2 (b) concentration.

Model predictions are also shown in fig. 2(a) and (b), obtained by fitting eqns. (1)–(4) with boundary conditions given by eqns. (8)–(9). In all cases (also those not shown in fig. 2) the model was able to get a close fit, especially for the water measurements. Fitted values of D (D_{diff} + D_{mech}) as a function of u are shown in fig. 3(a) for NaCl and 3(b) for O_2.

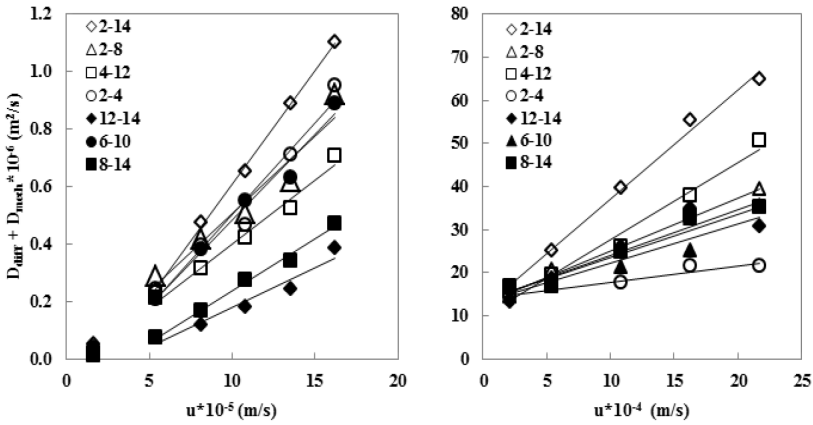

Figure 3: Calculated values of D_{diff} + D_{mech} based on (a) NaCl and (b) O_2 concentration, as a function of pore fluid velocity (u).

For solute dispersion, the u – D_{mech} relationship is linear for $u > 5 \cdot 10^{-5}$ m s^{-1}. Below this velocity the slope of the relationship approaches zero. For O_2 measurements the u – D_{mech} relationship is linear for $u > 2 \cdot 10^{-4}$ m s^{-1}. Below this velocity there is considerable scatter in the gas dispersion data, likely because the contribution by mechanical dispersion (D_{mech}) becomes small compared to molecular diffusion (D_{diff}), making it difficult to get a consistent and accurate determination of D_{mech}. The u–D curves for oxygen transport intercept the D-axis at a D-value of approximately $15 \cdot 10^{-6}$ m^2 s^{-1}, which represents D_{diff} for gas transport. In comparison the u–D relationship for chloride transport intercept the D-axis at a value close to zero, indicating that for the chloride transport D_{diff} can be neglected. Fig. 3 also shows that the slope (representing dispersivity, α) of the linear parts of the u – D_{mech} relationship for both NaCl and O_2 increases with increasing R in agreement with earlier observations [32].

Values of α were determined for each fluid type and particle size fraction. The resulting α-values are given in table 1. Fig. 4(a) and 4(b) show α-values for the NaCl (α_w) and for the O_2 (α_g) measurements respectively, as a function of R and D_m.

More gradual and less marked increase is exhibited from α_w for increasing R. Values range between 2.8 and 7.9 mm. More regular and evident increase is exhibited from α_g for increasing R, ranging between 3.8 and 25.5 mm. This is likely because increasing R causes increasing pore network tortuosity, and thus,

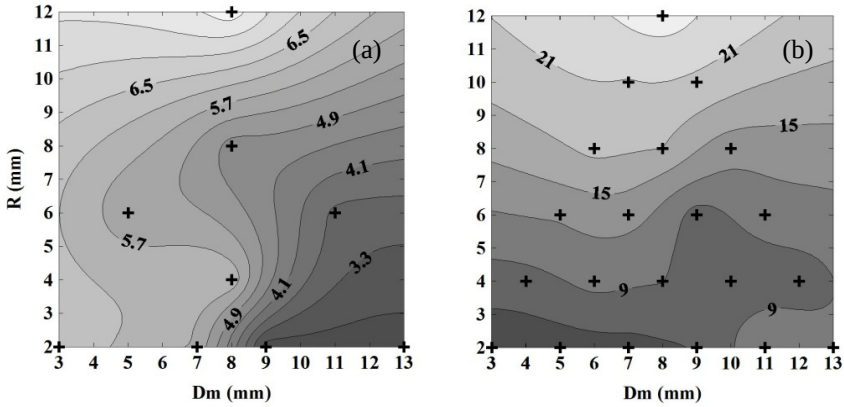

Figure 4: Contour plot of α as a function of D_m and R, for (a) NaCl and (b) O_2.

increasing dispersion [32, 33]. The α – D_m relationship is somewhat more complex but α is generally largest for small values of D_m, for both NaCl and O_2. Fig. 5 shows the ratio α_g/α_w as a function of D_m and R, with values ranging between 0.56 and 3.81.

The α_g/α_w ratio shows no consistent relationship with neither D_m nor R, although there is a tendency that α_g/α_w is lowest for low D_m and R values. More data, however, are needed to verify this tendency. On average α_g/α_w = 2.18 for the 9 particle size fraction in fig. 5. This value is very likely medium dependent and additional measurements of dispersion in other media are therefore required to assess medium dependency.

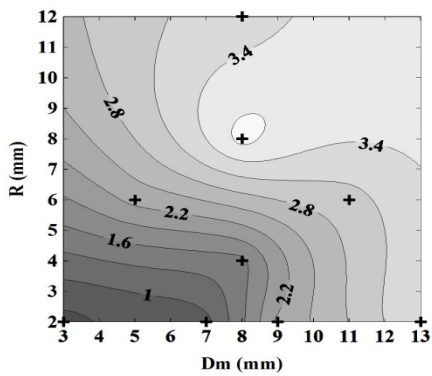

Figure 5: Contour plot of α_g/α_w, as a function of D_m and R.

5 Conclusions

Solute and gas dispersion were determined by analysing tracer breakthrough curves measured in gravel using chloride and oxygen as tracers. Measurements

were conducted using different flow velocities ranging from $1.6 \cdot 10^{-5}$–$1.6 \cdot 10^{-4}$ m s^{-1} for solute and from $2.2 \cdot 10^{-4}$–$2.2 \cdot 10^{-3}$ m s^{-1} for gas, both covering the identical Reynolds range. Results indicated that, for the same fluid pressure gradient across the columns, measurements of the solute tracer breakthrough curve takes about 12 times longer than gas. Both solute and gas dispersion coefficients (D_{mech}) showed an almost linear increase with fluid pore velocity (u) except at very low velocities. This is in agreement with earlier studies.

Dispersivity values (α_g and α_w) were determined as the slopes of the best fit straight lines to the linear parts of the u – D_{mech} relationships. A less marked increase of α_w with R was observed in solute measurements. An evident increase of α_g with R was shown for gas measurements, in agreement with earlier findings. This general trend is explained by considering the pore network tortuosity, which increases with R generating therefore greater α values. The relationship between α and D_m for both NaCl and O_2 was somewhat more complex but α was generally largest for small values of D_m.

Values of α_g (gas) were generally higher than α_w (solute), and the average ratio α_g/α_w was 2.18. Thus, gas dispersion coefficients generally increase faster with gas velocity than solute. Further investigations in other media are needed to fully understand the relationship between α_g/α_w, D_m and R.

References

[1] Thomson, N.R., Sykes, J.F., Van Vliet, D., A numerical investigation into factors affecting gas and aqueous phase plumes in the subsurface. *Contam. Hydrol*. **28(1-2)**, pp. 39-70, 1997.

[2] Silva, O., Grifoll, J., Non-passive Transport of Volatile Organic Compounds Infiltrated from a Surface Disk Source. *Transport in Porous Media* **77(1)**, pp. 103-129, 2009.

[3] Lewis, J., Sjostrom, J., Optimizing the experimental design of soil columns in saturated and unsaturated transport experiments. *Contam. Hydrol.* **115(1-4)**, pp. 1-13, 2010.

[4] Parkinson, R.J., Griffiths. P., Heathwaite, A.L., Transport of nitrogen in soil water following the application of animal manures to sloping grassland. *Hydrological Sciences Journal* **45(1)**, pp. 61-73, 2000.

[5] Wang. F., Ward. I.C., Radon entry, migration and reduction in houses with cellars. *Building and Environment* **37(11)**, pp. 1153-1165, 2002.

[6] Arands, R., Lam, T., Massry, I., Berler, D.H., Muzzio, F.J., Kosson, D.S., Modeling and experimental validation of volatile organic contaminant diffusion through an unsaturated soil. *Water Resources Res.* **33(4)**, pp. 599-609, 1997.

[7] Atteia, O., Hohener, P., Semianalytical model predicting transfer of volatile pollutants from groundwater to the soil surface. *Environmental Science e Technology* **44(16)**, pp. 6228-6232, 2010.

[8] El-Fadel, M., Findikakis, A.N., Leckie, J.O., Environmental impacts of solid waste landfilling. *J. Environ. Manag*. 50(1), pp. 1-25, 1997.

[9] De Visscher, A., Thomas, D., Boeckx, P., Van Cleemput, O., Methane oxidation in simulated landfill cover soil environments. *Environ. Sci. Technol.* 33(11), pp. 1854-1859, 1999.
[10] Liang, Y.K., Quan, X., Chen, J.W., Chung, J.S., Sung, J.Y., Chen, S., Xue, D.M., Zhao, Y.Z., Long-term results of ammonia removal and transformation by biofiltration. *J. Hazard. Mater.* 80(1-3), pp. 259-269, 2000.
[11] Pangala, S.R., Reay, D.S., Heal, K.V., Mitigation of methane emissions from constructed farm wetlands. *Chemosphere* **78(5)**, pp. 493-499, 2010.
[12] Pennock. D., Yates, T., Bedard-Haughn, A., Phipps, K., Farrell, R., McDougal, R., Landscape controls on N(2)O and CH(4) emissions from freshwater mineral soil wetlands of the Canadian Prairie Pothole region. *Geoderma* **155(3-4)**, pp. 308-319, 2010.
[13] Schaufler, G., Kitzler, B., Schindlbacher. A., Skiba, U., Sutton, M.A., Zechmeister-Boltenstern, S., Greenhouse gas emissions from European soils under different land use: effects of soil moisture and temperature. *European Journal of Soil Science* **61(5)**, pp. 683-696, 2010.
[14] Fukumoto, Y., Osada, T., Hanajima, D., Haga, K., Patterns and quantities of NH3, N2O and CH4 emissions during swine manure composting without forced aeration - effect of compost pile scale. *Bioresource technology* **89(2)**, pp. 109-114, 2003.
[15] Thummes, K., Kaempfer, P., Jaeckel, U., Temporal change of composition and potential activity of the thermophilic archaeal community during the composting of organic material. *Systematic and applied microbiology* **30(5)**, pp. 418-429, 2007.
[16] Bear, J., On the tensor form of dispersion in porous media. *J. Geophys. Res.* **66(4)**, pp. 1185-1197, 1961.
[17] Whitaker S., Diffusion and dispersion in porous media. *AICHE J.* **13(3)**, pp. 420-432, 1967.
[18] Greenkor R.A., Kessler D.P., Dispersion in heterogeneous nonuniform anisotropic porous media. *Ind. Eng. Chem.* **61(5)**, pp. 8-15, 1969.
[19] Scheidegger A.E., *The physics of flow through porous media, 3rd edn.* University of Toronto Press, 1974.
[20] Brenner H., Dispersion resulting from flow through spatially periodic porous-media. *Philos. T. Roy. Soc. A.* **297(1430)**, pp. 81-133, 1980.
[21] Gelhar L.W., *Stochastic subsurface hydrology*, Prentice-Hall, 1993.
[22] Sinclair, R.J., Potter, O.E., Dispersion of gas in flow through a bed of packed solids. *Trans. I. Chem. E.* **43(1)**, pp. T3-T9, 1965.
[23] Evans, E.V., Kenney, C.N., Gaseous dispersion in packed beds at low Reynolds numbers. *Trans. Inst. Chem. Engr.* **44(6)**, pp. T189-T197, 1966.
[24] Edwards, M.F., Richards, J.F., Gas dispersion in packed beds. *Chem. Eng. Sci.* **23(2)**, pp. 109-123, 1968.
[25] Suzuki, M., Smith J.M., Dynamics of diffusion and adsorption in a single catalyst pellet. *AICHE J.* **18(2)**, pp. 326-333, 1972.

[26] Coelho, M.A.N., Guedes de Carvalho, J.R.F.G., Transverse dispersion in granular beds. 1. Mass transfer from a wall and the dispersion coefficient in packed beds. *Chem. Eng. Res. Des.* **66(2)**, pp. 165-177, 1988.
[27] Tan, C.S., Liou D.C., Axial dispersion of supercritical carbon dioxide in packed beds. *Ind. Engng. Chem. Res.* **28(8)**, pp. 1246-1250, 1989.
[28] Poulsen, T.G., Suwarnarat, W., Hostrup, M.K., Kalluri, P.N.V., Simple and rapid method for measuring gas dispersion in porous media: methodology and applications. *Soil Sci.* **173(3)**, pp. 169-174, 2008.
[29] Delgado, J.M.P.Q., A critical review of dispersion in packed beds. *Heat and Mass Transf.* **42(4)**, pp. 279-310, 2006.
[30] Gidda, T., Cann, D., Stiver, W.H., Zytner, R.G., Airflow dispersion in unsaturated soil. *J. Contam. Hydrol.* **82(1-2)**, pp. 118-132, 2006.
[31] Bromly, M., Hinz, C., Aylmore L.A.G., Relation of dispersivity to properties of homogeneous saturated repacked soil columns. *European Journal of Soil Science* **58(1)**, pp. 293-301, 2007.
[32] Sharma, P., Poulsen, T.G., Gas dispersion and immobile gas volume in solid and porous particle biofilter materials at low air flow velocities. *Journal of the Air & Waste Management Association* **60(7)**, pp. 830-837, 2010.
[33] Pugliese, L., Poulsen, T.G., Andreasen, R.R., Relating gas dispersion in porous media to medium tortuosity and anisotropy ratio. *Water Air and Soil Pollution* **223(7)**, pp. 4101-4118, 2012.
[34] Hiby, J.W., Longitudinal and transverse mixing during single-phase flow through granular beds. *Institution of Chem. Engrs*., pp. 312-325, 1962.
[35] Miller, S.F., King, C.J., Axial dispersion in liquid flow through packed beds. *AIChE J.* **12(4)**, pp. 767-773, 1966.
[36] Klotz, D., Moser, H., Hydrodynamic dispersion as aquifer characteristic, model experiments with radioactive tracers. *Isotope Techn. Groundwater Hydrology*, pp. 341-355, 1974.
[37] Guedes de Carvalho, J.R.F.G., Delgado, J.M.P.Q., Effect of fluid properties on dispersion in flow through packed beds. *AIChE J.* **49(8)**, pp. 1980-1985, 2003.
[38] Herrera, P.A., Massabo, M., Beckie, R.D., A meshless method to simulate solute transport in heterogeneous porous media. *Advances in Water Resources* **32(3)**, pp. 413-429, 2009.
[39] Hamamoto, S., Moldrup, P., Kawamoto, K., Komatsu, T., Rolston, D.E., Unified measurement system for the gas dispersion coefficient, air permeability, and gas diffusion coefficient in variably saturated soil. *Soil Science Society of America Journal* **73(6)**, pp. 1921-1930, 2009.
[40] Hunt, A.G., Skinner, T.E., Predicting dispersion in porous media. *Complexity* **16(1)**, pp. 43-55, 2010.